Available online at www.sciencedirect.com
ScienceDirect
Journal of Bionic Engineering 4 (2007) 165−176

Simulation of Fluid Flow in a Channel Induced by Three Types of Fin-Like Motion

Wojciech Kowalczyk, Antonio Delgado

Institute of Fluid Mechanics, *University of Erlangen-Nuremberg*, *Cauerstr*. 4, *D*-91058 *Erlangen*, *Germany*

Abstract

One of many interesting research activities in biofluidmechanics is dedicated to investigations of locomotion in water. Some of propulsion mechanisms observed in the underwater world are used in the development process of underwater autonomic vehicles (AUV). In order to characterise several solutions according to their manoeuvrability, influence on the surrounding fluid and energetic efficiency, a detailed analysis of fin-like movement is indispensable.

In the current paper an analysis of undulatory, oscillatory and combined fin-like movements by means of numerical simulation is carried out. The conservation equation of mass and the conservation equation of momentum are solved with the Finite Volume Method (FVM) by use of the software CFX−10.0. The undulatory and oscillatory fin movements are modelled with an equation that is implemented within an additional subroutine and joined with the main solver. Numericalsimulations are carried out in the computational domain, in which one fin is fixed in a flow-through water duct. Simulations are carried out in the range of the *Re* number up to 10^5. The results show significant influence of applied fin motion on the velocity distribution in the surrounding fluid.

Keywords: biofluid dynamics, fin-like movement, fish propulsion, computational fluid dynamics

1 Introduction

The evolution of life on the earth, which has begun in water, has provided for a diversified spectrum of possible locomotion solutions by underwater organisms (e.g. see Ref. [1]). Various aspects of fish locomotion are discussed in numerous publications world wide[2–11].

Liao *et al.*[12] and Müller[13] reported that some sea inhabitants use natural environment or by themselves produced vortex systems to move with higher energetic efficiency. As an example fish living in swarms are studied. The supporting effect of surrounding fluid flow on swimming efficiency is deduced by means of reduced muscle activity.

Wardle[14] as well as Wardle and Videler[15] investigated the maximum swimming speed of fish. The authors observed that fish are able to exceed a theoretically determined maximum speed applying different swimming kinematics under purposeful use of the flow conditions in their environment.

The theoretical and experimental analysis of the kinetics and the coordianation of a multi-fin system were carried out for *Ostracion meleagris camurum*[16] and *Chilomycterus schoepfi*[17]. Harris[18] examined the meaning of the position and movement of in pairs coordinated fins for the balance and the translational movement of shark and bone fish.

As a very important component of the underwater locomotion, the manoeuvring ability of fish is described in literature. Webb[19] defined the manoeuvre as a series of changes of the direction and position of a fish for reaching one given place in space.

The kinematics and performance of the manoeuvring system of several bone fish were compared by Walker[20] in an overview article. Beyond that, Weihs[21] analyzed the oppositeness of the simultaneous

Corresponding author: Wojciech Kowalczyk
E-mail: kowalczyk@lstm.uni-erlangen.de

realization of stability and manoeuvrability in locomotion systems under water. Drucker and Lauder[22] investigated the mobility of sunfish and observed the differences in the flow field during steady translational and rotational movements. The characteristic of the jet-propulsion according to its dynamics and manoeuvrability was described by Korde[23], Park *et al.*[24] and Mohseni[25].

A step toward biomimetics was undertaken by Bandyopadhyay[26]. Basing on investigations of the fish manoeuvrability the author developed an underwater vehicle, whose swimming characteristics is similar to the natural object.

Blake[27] and Sfakiotakis *et al.*[28] gave meanwhile a good overview of the propulsion systems used by fish. The authors differentiated in particular between solutions that enable high accelerations (e.g. thunfish) and those that aim at manoeuvring abilities.

In addition to the variety of propulsion mechanisms for pure translation and rotation, there are some locomotion solutions in sea biotopes, which aim at precise manoeuvre in a quite difficult terrain as well as optimised emissions and influence on the environment in order not to wake the hunt instinct of other sea inhabitants. Thus, the anatomy of such organisms enables production of small forces due to low ratio of locomotive active (fins) and passive parts. To this category belongs the sea horse, whose translational movement is caused by synchronous kinematics of dorsal and pectoral fins undulating with the frequency up to 50 Hz[29]. Concerning the locomotion of sea horse, the pioneer works on this field were carried out by Breder and Edgerton[30]. In Fig. 1 the characteristic of sea horses undulatory fin

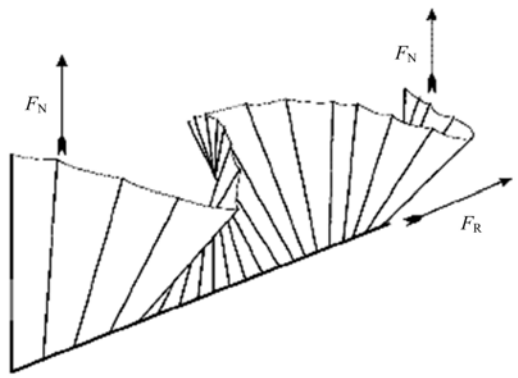

Fig. 1 Undulatory fin movement of a sea horse[25].

movement can be seen.

Lourie *et al.*[31] and Kuiter[32] contributed meanwhile to the biological classification of all known sea horses. The mechanical characteristics of the dorsal fin of *Hippocampus* were investigated by Ashley-Ross[33]. This authoress calculated mechanical stresses in muscles as a function of the temperature and the achieved performance by different fin frequencies. A further analysis of the speed of muscle contractions in the dorsal fin of a sea horse was carried out by Bergman[34].

Sfakiotakis *et al.*[35] experimentally modeled the kinetics of a dorsal fin with the help of an accordingly moved membrane. Furthermore, Blake[29] investigated the translational movement of a sea horse by means of the cinematography. This author measured forces produced by pectoral and dorsal fins and analysed different translational and rotational arts of sea horse movement.

Fundamental theoretical aspects of the biofluid dynamics of swimming according to the undulatory and/or oscillatory fin movement were treated in the articles of Lighthill and Blake[36] and Daniel *et al.*[37] as well as in numerous further works, e.g. [38–41].

Sfakiotakis *et al.*[35] and Consi *et al.*[42] modeled the kinetics of a dorsal fin of sea horse. Nevertheless, both authors recommended further analysis of the movement of all active parts on the basis of three-dimensional observations. A better understanding of the interaction between stabilisation and locomotion systems should be attained. This is an essential requirement for biomimetical design of autonomous underwater vehicles (AUV) basing on a sea horse-like propulsion system.

Wu[43] introduced into scaling problems of the locomotion of microorganisms and fish at different Reynolds numbers. The investigations were based on comparative analysis of zoological and dynamical similarities. Additionally, McHenry and Lauder[44] investigated scale-up phenomena of coasting in zebrafish during its growth phase.

Mittal[45] reported on numerical methods used for simulations of a translational movement under water. This author presented an overview of possibilities and restrictions of several numerical procedures according to the computation on the biofluid dynamics. Apart from the simulation with RANS (Reynolds Averaged Navier

Stokes) the Direct Numerical Simulation (DNS), the Large Eddy Simulation (LES) and the Detached Eddy Simulation (DES) were addressed.

From the modelling point of view, further aspect becomes central meaning, i.e. an interactive effect of moving body parts and flow of surrounding fluid (Fluid Structure Interaction – FSI). This topic was discussed by Gilmanov and Sotiropoulos[46]. They described three-dimensional numerical investigations of biotic and abiotic bodies immersed in water, i.e. a ball, a fish (mackerel) and a copepod. Leroyer and Visonneau[47] dealed with the fish movement with the help of numerical simulation based on RANS. Further publications examined abilities of the Immersed Boundary Finite Volume Method (IBFVM) for numerical simulations of immersed complex geometries[48,49] and the Immersed Finite Element Method (IFEM) for the CFD-prediction in biological systems[50].

The current paper contributes to the investigations of biomechanical aspects of propulsion systems in water. Due to preliminary phase of the present study, an extended survey of literature according to fin-like motion and numerical methods is presented. By means of computational fluid dynamics the influences of oscillatory and undulatory fin movements on the surrounding fluid are studied.

2 Governing equations

In the current paper the equation system is based on the conservation of mass and momentum[51]. The conservation equation of mass for incompressible substances expressed in the form of the Cartesian tensor is written as

$$\frac{\partial u_i}{\partial x_i} = 0, \tag{1}$$

where u_i denotes the velocity and x_i the direction. The conservation equation of momentum for incompressible fluids with constant viscosity and without influence of volume forces (i.e. gravitational force) can be written as

$$\rho\left[\frac{\partial u_i}{\partial t} + u_j \frac{\partial u_i}{\partial x_j}\right] = -\frac{\partial p}{\partial x_i} + \mu \frac{\partial^2 u_i}{\partial x_j \partial x_j}. \tag{2}$$

Hereby, p indicates the pressure, μ the dynamic viscosity, t the time and j as well as i the direction index ($i, j = 1, 2, 3$).

3 Methods

The governing equations are solved with the Finite Volume Method (FVM) using the commercial software CFX−10.0 (ANSYS CFX). The implicit backward Euler method is used for time discretisation. The pressure-velocity coupling is realised with the SIMPLE algorithm[51]. Numerical calculations are regarded as sufficiently converged if the RMS convergence takes values smaller than 1.0×10^{-4}. Simulations take approximately 1.0×10^5 s of CPU time on a serial Intel Xeon 64-bit processor.

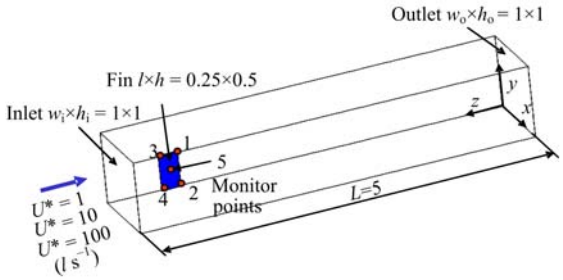

Fig. 2 Computational domain.

Numerical simulations are carried out for the fluid flow in a duct with following characteristic dimensionless lengths (width/$w_{i,o}$ × height/$h_{i,o}$ × length/L = 1×1×5). The properties of the liquid correspond to that of water at 25 ˚C. In the channel an infinite and impermeable thin plate – a fin – with dimensions (length/l × height/h = 0.25×0.5) is localised at the distance of 0.5 from the inlet patch. In the computational domain (see Fig. 2) an unstructured moving grid with 1.7×10^6 tetrahedrons is generated using ICEM ANSYS. Slip boundary conditions are applied at the walls of the channel in order to decrease their influence on the fluid flow. Additionally, a constant velocity at the inlet, the ambient pressure at the outlet plane and no slip boundary condition on the fin surface are implemented. Using an equation

$$\vec{w} = f(x,y,z,t) = D(x,y,z)\cdot A\cdot(\sin \omega t), \tag{3}$$

an undulatory and oscillatory fin-like movement is defined. In order to avoid deformation at the beginning of the fin (e.g. a place where dorsal fin of a sea horse is consolidated with the main body) the above mentioned equation contains linear damping factor (D) along the

z-axis

$$D(x,y,z) = \mathrm{c} \cdot z(x,y) + z_0 . \quad (4)$$

The fin-like motion is described within additional subroutines coupled with the main solver.

In Eqs. 3−4 used for description of fin movement, x, y and z denote the location in the coordinate system, A the amplitude of 0.01 and ω the frequency of 3 s^{-1}. In order to ensure an expected effect of Eqs. 3−4 on the fin, i.e. zero deformation at the beginning and maximal deformation at the end of the fin, following values of constants c (c = −4) and z_0 (z_0 = 18) are applied. The values of c and z_0 depend on the dimension and on the localisation of the fin in the channel. The velocity vector $\vec{U}_{\mathrm{init}} = 0$ is implemented as initial conditions in the whole computational domain except the inlet patch. Transient numerical simulations are carried out for the total time of 12 s using the constant time step of 8×10^{-2} s.

Since the Reynolds numbers $Re = \rho\, U_{\mathrm{inlet}}\, l\, \mu^{-1}$ are considered in the range of $O(10^3-10^5)$, the numerical model contains the Shear Stress Transport Model (SSTM) in order to model the turbulence.

The SSTM of Menter[52] combines properties of the Launder and Spalding's k-ε model[53] for the bulk flow and the Wilcox's k-ω model[54,55] at the wall. In this model applying advanced near-wall treatment enables accurate calculations in regions close to walls for different grid densities. The validation of the SSTM is described by Bardina *et al*.[56].

The numerical simulations are carried out for three cases of the fin-like movement: i) undulatory (see Fig. 3a), ii) oscillatory (see Fig. 3b) and iii) combined (see Fig. 3c). Hereby, both the undulatory and oscillatory fin-like motions are realised in the xz-plane and the combined fin-like movement consist of undulatory motion in the xz-plane and oscillatory motion in the xy-plane. The first and third movements correspond to a dorsal fin motion of sea horse and the second complies with a caudal fin motion of fish. Fig. 4 shows an example of an undulatory deformed fin. The investigations are carried out with the inlet velocity of fluid U_{inlet} of 1, 10 and 100 l s^{-1}, where 1 l s^{-1} = 0.25 m·s^{-1}, for all three cases of fin-like motion.

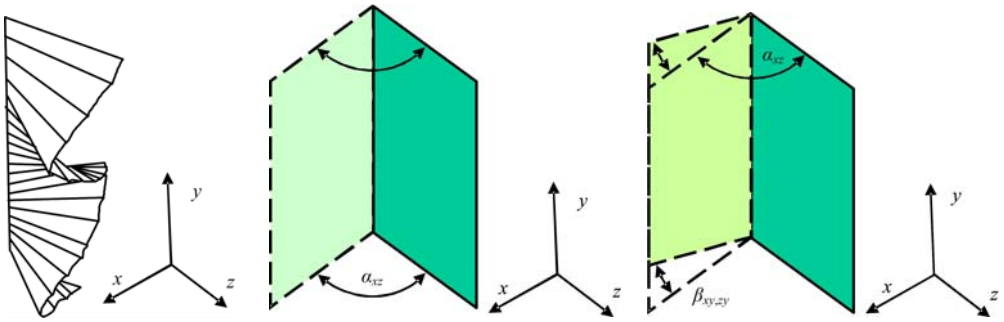

(a) undulatory (b) oscillatory (c) combined

Fig. 3 Scheme of the considered fin-like movements.

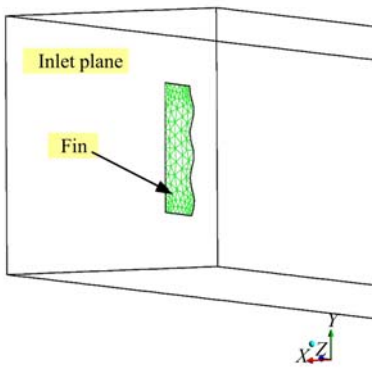

Fig. 4 Example of fin deformation and mesh on the fin surface.

4 Results

In the current paper the influences of different fin-like movements on the surrounding fluid were studied. As already mentioned, numerical simulations are started with the initial velocity $\vec{U}_{\mathrm{init}} = 0$ and inlet velocity of fluid applied at the inlet patch. As first, results of the undulatory fin-like movement are shown. Fig. 5a and Fig. 5b illustrate the velocity distribution of the undulatory fin-like motion for the inlet velocity U_{inlet} = 1 l s^{-1} and U_{inlet} = 10 l s^{-1} respectively. The velocity distribution for 100 l s^{-1} has very similar character to that for

10 $l\ s^{-1}$, therefore it has not been presented in the current paper. In Fig. 5a a characteristic velocity distribution for undulatory fin-like movement can be observed. Since the initial velocity in the computational domain equals zero, the most significant influence of fin movement on the surrounding fluid can be observed during the initial stage of calculation. It can be recognised with bright (0.245 $m{\cdot}s^{-1}$) and dark (0.255 $m{\cdot}s^{-1}$) fields in the velocity distribution. After approximately five seconds the fluid flow close to the fin stabilises, due to vanishing influence of $\vec{U}_{\text{init}} = 0$ and the fin movement does not influence the surrounding fluid significantly. Solely a trace with the value (0.248 $m{\cdot}s^{-1}$) that is slightly smaller than the inlet velocity can be seen. The higher inlet velocity U_{inlet} = 10 $l\ s^{-1}$ (2.5 $m{\cdot}s^{-1}$) causes much faster building of the fully developed velocity distribution in the duct that leads to a single trace with value up to 2.498 $m{\cdot}s^{-1}$.

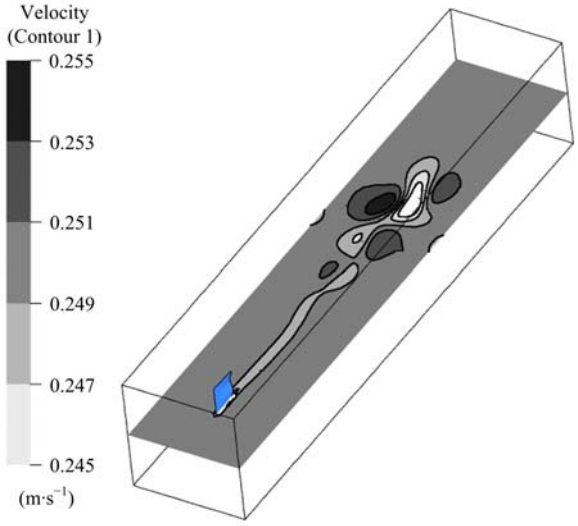

(a) Inlet velocity 0.25 $m{\cdot}s^{-1}$

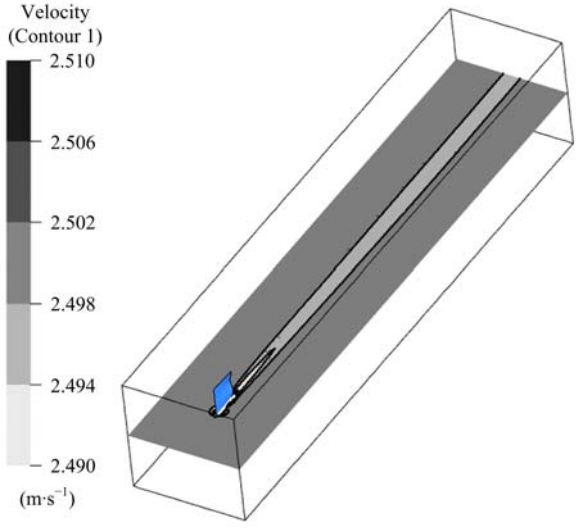

(b) Inlet velocity 2.5 $m{\cdot}s^{-1}$

Fig. 5 The velocity distribution in the channel during undulatory fin-like movement.

The velocity distributions can also be presented in the form of isosurfaces. Fig. 6a and Fig. 6b show isosurfaces for the velocity of fluid after 12 s. The results reveal that there is no typical von Karman vortex street in such a case. Large vortex structures developed at the beginning of the simulation become smaller with time. This behaviour corresponds very well to the velocity distribution presented in Fig. 5.

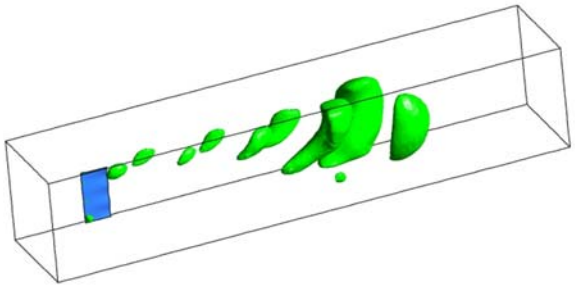

(a) Inlet velocity 0.25 $m{\cdot}s^{-1}$ (isosurface for the velocity 0.251 $m{\cdot}s^{-1}$)

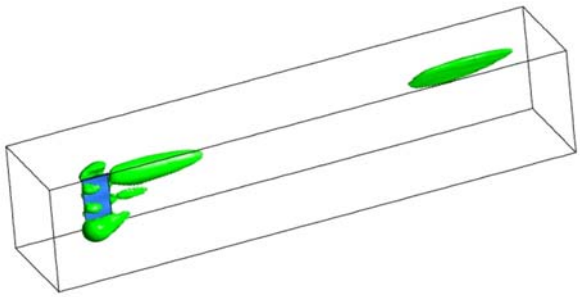

(b) Inlet velocity 2.5 $m{\cdot}s^{-1}$ (isosurface for the velocity 2.501 $m{\cdot}s^{-1}$)

Fig. 6 Isosurfaces of the velocity during undulatory fin-like movement.

Fig. 7 shows undulatory fin displacement registered in monitor points P1–P5. Since points P3 and P4 are localised at the beginning of the fin and do not move due to applied damping function, the displacement in points P1, P2 and P5 can be noted as a wave with different amplitude in each point. The highest fin displacement of 1.8×10^{-3} m is registered in monitor point P1. The fin dislocation in point P2 amounts 0.6×10^{-3} m and in the middle of the fin (P5) a slight decrease from 0.5×10^{-3} m to 0.3×10^{-3} m is observed.

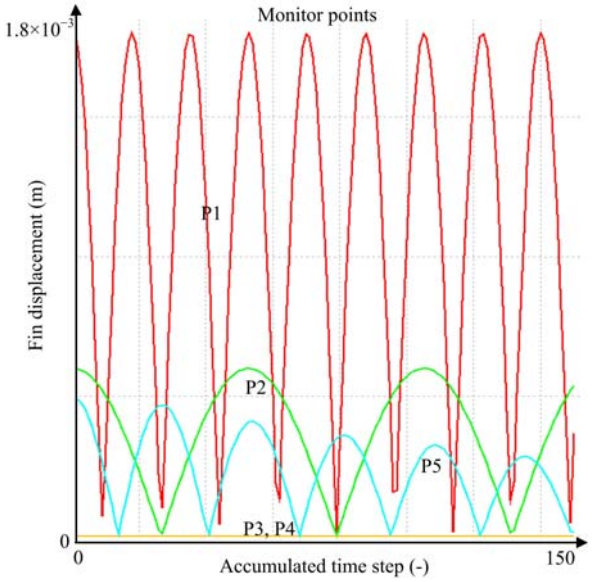

Fig. 7 The fin displacement in monitor points during undulatory fin-like motion.

In the second investigated case of the fin-like movement, an oscillatory motion of the inflexible plate in the channel was investigated. Fig. 8 visualises the velocity distribution. For the inlet velocity, U_{inlet} = 1.0 l s^{-1}, already at the beginning of simulation the characteristic von Karman vortex street can be clearly seen. In comparison with the velocity distribution in Fig. 5 very big differences between the two fin systems can be seen. Such different fluid flow also indicates big differences in the momentum transfer from the fin to the surrounding water. Consequently different energy consumption, efficiency and locomotive characteristic of propulsion can be deduced. Whilst small influence on fluid by the undulatory system allows an efficient propulsion system for small transport velocities, the oscillatory fin-like motion enables higher accelerations and transitional velocities by higher energy effort. These results well cover biological observations in the nature and experimental investigations in laboratories described in the literature.

The change of the inlet velocity from 1 l s^{-1} to 10 l s^{-1} significantly influences the velocity distribution. The channel length of L = 5 enables presentation of the fluid flow calculated during the last two seconds of the simulation. Nevertheless, two zones can be clearly recognised in the velocity distribution. They build a kind of

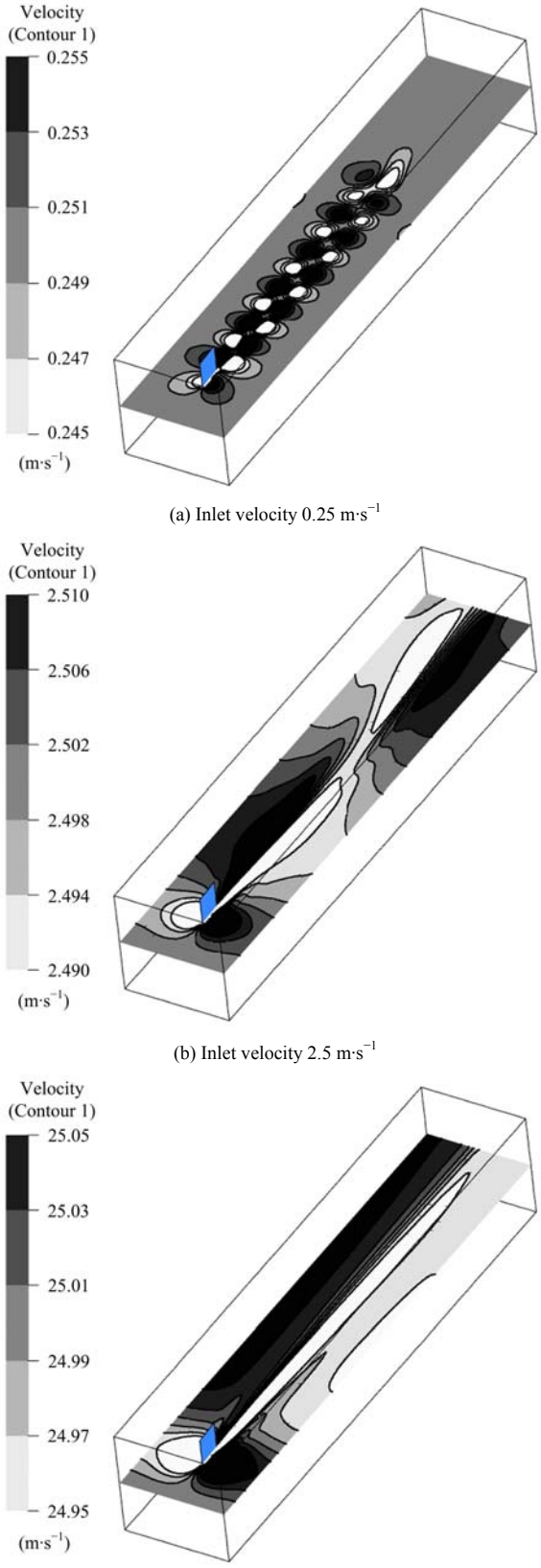

(a) Inlet velocity 0.25 m·s^{-1}

(b) Inlet velocity 2.5 m·s^{-1}

(c) Inlet velocity 25 m·s^{-1}

Fig. 8 The velocity distribution in the channel during oscillatory fin-like movement.

an expanded vortex street. If the inlet velocity is set to 100 $l\ s^{-1}$, the velocity distribution in the range of 25.05 $m{\cdot}s^{-1}$ to 24.95 $m{\cdot}s^{-1}$ in Fig. 8c shows only a part of the one vortex zone. However, the effect of the oscillatory fin-like movement causing characteristic velocity fields with minimal and maximal velocity can be seen.

In Fig. 9 the isosurfaces for the same velocities in the case of undulatory fin-like movement (compare to Fig. 6) are visualised. Characteristic flow patterns identified in the velocity distribution are confirmed with the help of three dimensional structures. First of all the spatial organization of the fields that belong to the von Karman vortex street by the inlet velocity 1 $l\ s^{-1}$ can be clearly seen in Fig. 9a.

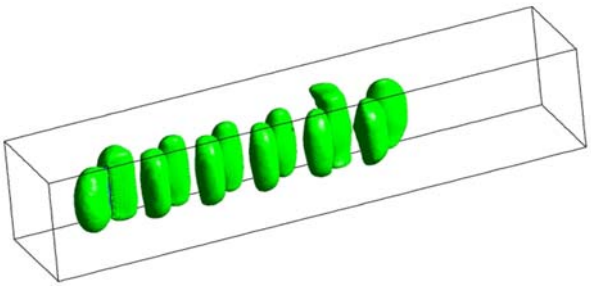

(a) Inlet velocity 0.25 $m{\cdot}s^{-1}$ (isosurface for the velocity 0.251 $m{\cdot}s^{-1}$)

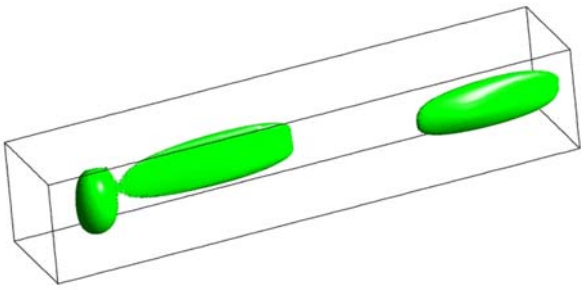

(b) Inlet velocity 2.5 $m{\cdot}s^{-1}$ (isosurface for the velocity 2.501 $m{\cdot}s^{-1}$)

Fig. 9 Isosurfaces of the velocity during oscillatory fin-like movement.

The change from undulatory to oscillatory fin-like movement has been also reflected in the motion registered in the monitor points (see Fig. 10). While monitor points P1 and P2 oscillate simultaneously only one curve indicating the displacement value of 2.4×10^{-3} m can be observed. The monitor point located in the fin centre P5 moves with the amplitude of 1.0×10^{-3} m.

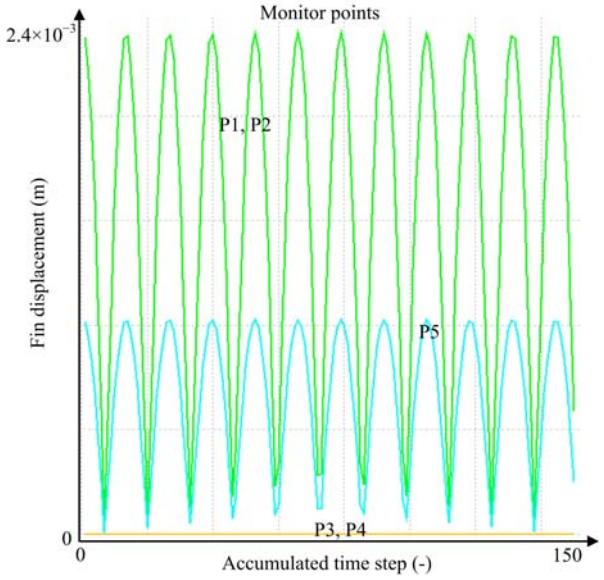

Fig. 10 The fin displacement in monitor points during oscillatory fin-like movement.

The third considered case consists of combined horizontal undulatory and vertical oscillatory fin-like movement. The velocity distributions for the inlet velocity 1 $l\ s^{-1}$ and 10 $l\ s^{-1}$ are depicted in Fig. 11. In both cases the dominating influence of the undulatory fin-like movement can be stated. This cognition can be confirmed by comparison with Fig. 5, where no significant differences with Fig. 11 are recognisable. A similar conclusion can be made comparing isosurfaces of the velocity in Fig. 12 and Fig. 6.

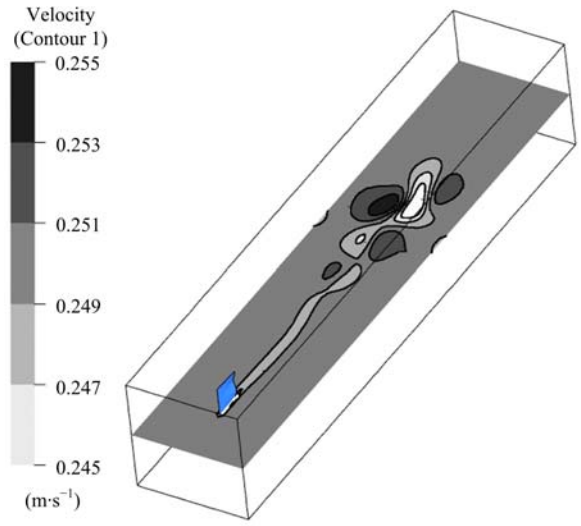

(a) Inlet velocity 0.25 $m{\cdot}s^{-1}$

Fig. 11 The velocity distribution in the channel during combined fin-like movement.

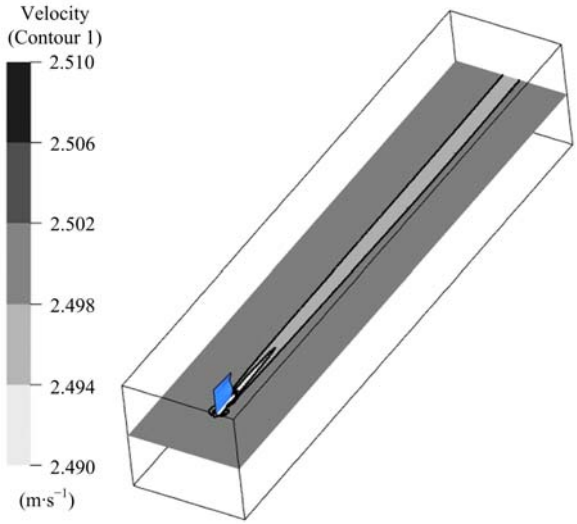

(b) Inlet velocity 2.5 m·s^{-1}

Fig. 11 Continued.

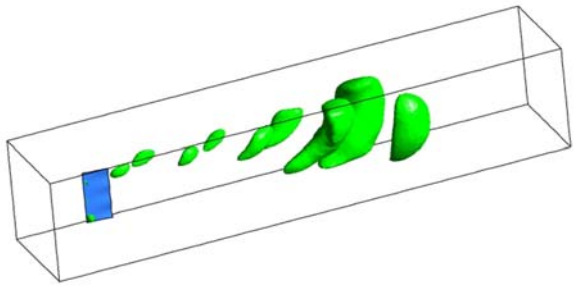

(a) Inlet velocity 0.25 m·s^{-1} (isosurface for the velocity 0.251 m·s^{-1})

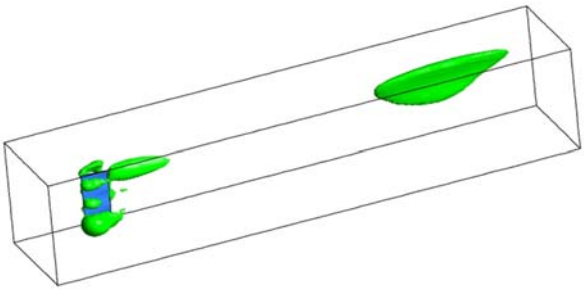

(b) Inlet velocity 2.5 m·s^{-1} (isosurface for the velocity 2.501 m·s^{-1})

Fig. 12 Isosurfaces of the velocity during combined fin-like movement.

The situation changes completely if the displacements of the control points are analysed. Fig. 13 shows the motion of the control points during combined fin-like motion. Comparisons with Fig. 7 and Fig. 10 reveal significant differences. The complex movement in P1 results in the maximal displacement of 3.3×10^{-3} m. In points P2 and P5 maximal values of 2.6×10^{-3} m and 1.1×10^{-3} m are noted respectively.

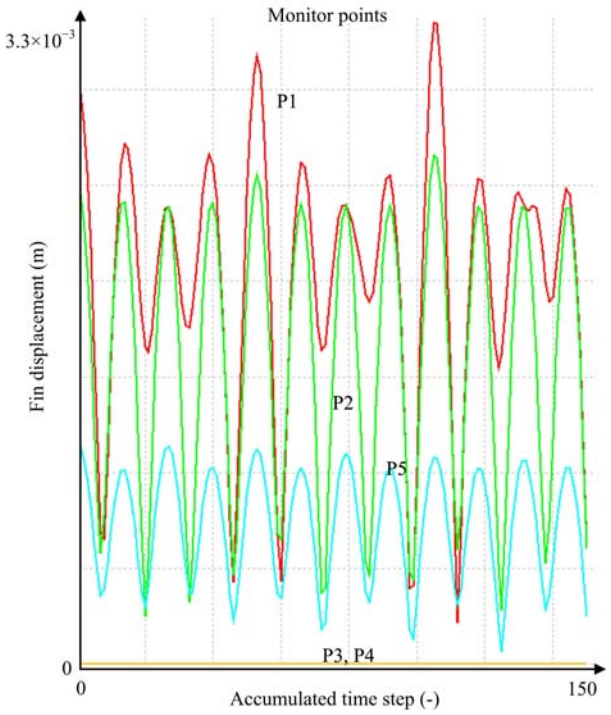

Fig. 13 The fin displacement in monitor points during combined fin-like movement.

Further differences between undulatory and oscillatory fin-like motions for the inlet velocity 1 *l* s^{-1} are illustrated in Fig. 14, where the velocity and shear strain rate run along arbitrary chosen lines. All four lines are parallel and start at the inlet path in following *x*, *y*, *z*-coordinates: Line 1 (0.6, 0.5, 5), Line 2 (0.25, 0.5, 5), Line 3 (0.5, 0.25, 5) and Line 4 (0.5, 0.75, 5). Additionally to higher values in the velocity distribution, which could be also observed in the previous figures, in the case of oscillatory fin-like movement approximately two times higher shear strain rates are stated in comparison with the undulatory fin-like motion.

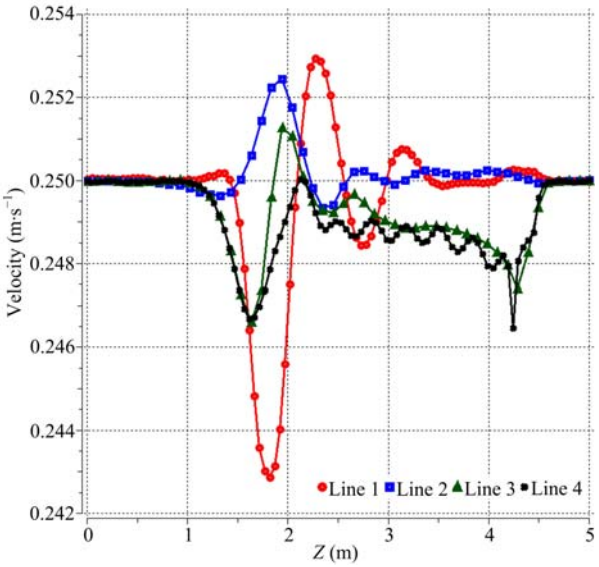

(a) Undulatory fin-like movement

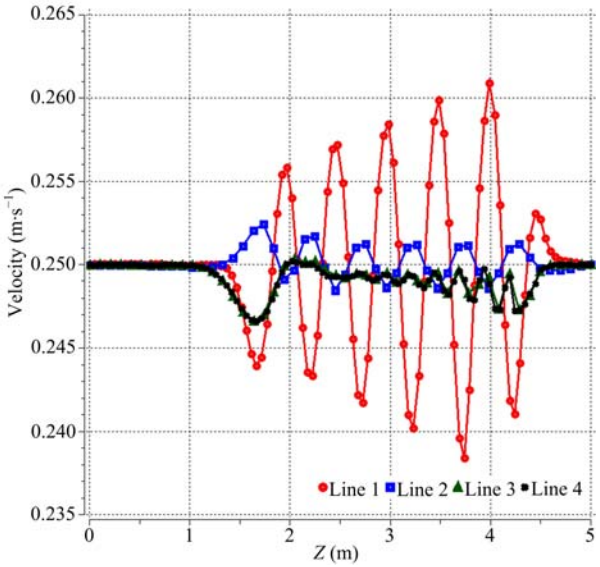

(b) Oscillatory fin-like movement

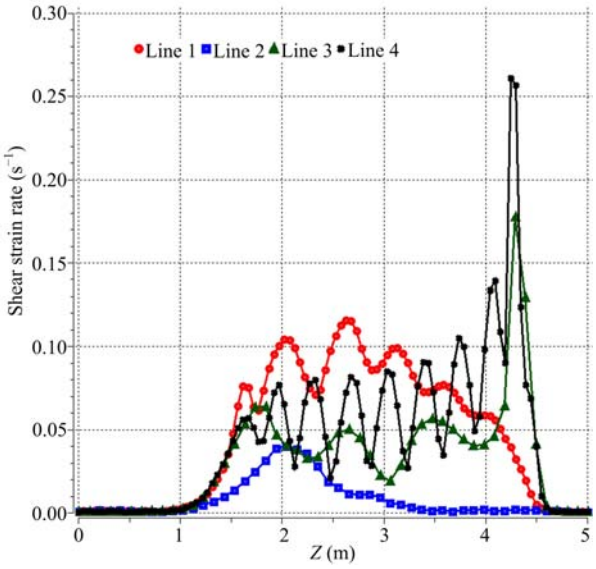

(c) Undulatory fin-like movement

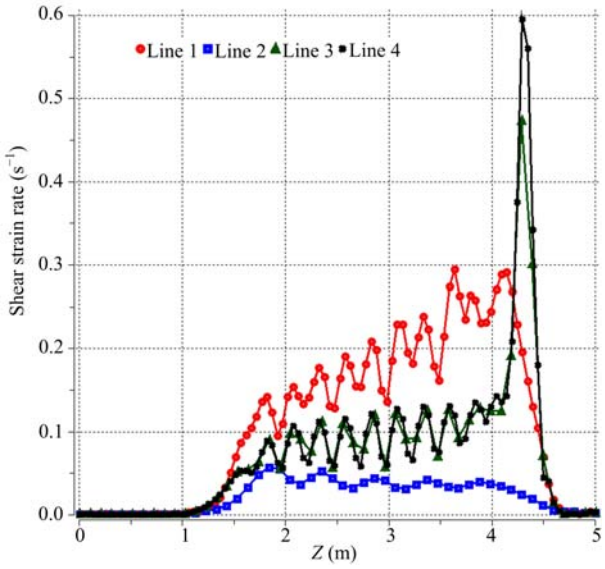

(d) Oscillatory fin-like movement

Fig. 14 The velocity and shear strain rate along the parallel lines in a duct.

5 Conclusions

In the current paper numerical studies of undulatory, oscillatory and combined fin-like movement are presented. The results clearly show that there are a lot of differences according to the influence of moving fin on the surrounding fluid. For the oscillatory fin-like movement a characteristic von Karman vortex street during the simulation can be observed. The undulatory and combined fin-like motions build bigger vortex structures only at the beginning of the simulation. With increasing simulation time the vortices become significantly smaller. These phenomena can be especially visible for the inlet velocity 1 l s^{-1}. The results correspond to the observations in the nature and laboratories that mentioned better ability of oscillatory system to produce higher velocities and accelerations and undulatory systems for energetically effective propulsion at

low velocities and required high level of manoeuvrability, e.g. sea horse. The undulatory fin-like motion causes also approximately two times smaller shear strain rates in comparison with the oscillatory system. Using monitor points located in the edges and in the middle of the fin, the characteristics of fin-deformation for all considered systems were investigated. The biggest deformation is noted for combined fin-like movement. Taking into account that the influence of the fin motion on the surrounding fluid correlates with the noise produced in a fluid, systems basing on the undulatory propulsion are supposed to be quieter. This hypothesis will be verified during planed experimental and numerical investigations in details.

Also further aspects from the numerical point of view like larger fin and mesh displacements as well as Fluid Structure Interaction (FSI) will be addressed. Moreover, Digital Particle Image Velocimetry (DPIV) and Electronic Specle Pattern Interferometry (ESPI) will be used in order to experimentally validate numerical predictions.

References

[1] Clack J A. From fins to fingers. *Science*, 2004, **304**, 57–58.

[2] Standen E M, Lauder G V. Dorsal and anal fin friction in bluegill sunfish (*Lepomis macrochirus*): Three-dimensional kinematics during propulsion and maneuvering. *Journal of Experimental Biology*, 2005, **208**, 2753−2763.

[3] Drucker E G, Lauder G V. Locomotor function of the dorsal fin in teleost fishes: Experimental analysis of wake forces in sunfish. *Journal of Experimental Biology*, 2001, **204**, 2943−2958.

[4] Drucker E G, Lauder G V. Function of pectoral fins in rainbow trout: Behavioral repertoire and hydrodynamic forces. *Journal of Experimental Biology*, 2003, **206**, 813−826.

[5] Lauder G V, Nauen J C, Drucker E G. Experimental hydrodynamics and evolution: Function of median fins in ray-finned fishes. *Integrative and Comparative Biology*, 2002, **42**, 1009−1017.

[6] Lauder G V, Drucker E G. Morphology and experimental hydrodynamics of fish fin control surfaces. *IEEE Journal of Oceanic Engineering*, 2004, **29**, 556−571.

[7] Triantafyllou M S, Techet A H, Hover F S. Review of experimental work in biomimetic oils. *IEEE Journal of Oceanic Engineering*, 2004, **29**, 585−594.

[8] Hover F S, Haugsdal Ø, Triantafyllou M S. Effect of angle of attack profiles in flapping foil propulsion. *Journal of Fluids and Structures*, 2004, **19**, 37−47.

[9] Barretti D S, Triantafyllou M S, Yue D K P, Grosenbaugh M A, Wolfgang M J. Drag reduction in fish-like locomotion. *Journal of Fluid Mechanics*, 1999, **392**, 183−212.

[10] Read D A, Hover F S, Triantafyllou M S. Forces on oscillating foils for propulsion and maneuvering. *Journal of Fluids and Structures*, 2003, **17**, 163−183.

[11] Triantafyllou M S, Techet A H, Zhu Q, Beal D N, Hover F S, Yue D K P. Vorticity control in fish-like propulsion and maneuvering. *Integrative Comparative Biology*, 2002, **42**, 1026−1031.

[12] Liao J C, Beal D N, Lauder G V, Triantafyllou M S. Fish exploiting vortices decrease muscle activity. *Science*, 2003, **302**, 1566−1569.

[13] Müller U K. Fish'n flag. *Science*, 2003, **302**, 1511−1512.

[14] Wardle C S. Limit of fish swimming speed. *Nature*, 1975, **255**, 725−727.

[15] Wardle C S, Videler J J. How do fish break the speed limit?. *Nature*, 1980, **284**, 445−447.

[16] Hove J R, O´Bryan L M, Gordon M S, Webb P W, Weihs D. Boxfishes (Teleostei: Ostraciidae) as a model system for fishes swimming with many fins: Kinematics. *Journal of Experimental Biology*, 2001, **204**, 1459−1471.

[17] Arreola V I, Westneat M W. Mechanics of propulsion by multiple fins: Kinematics of aquatic locomotion in the burrfish (*Chilomycterus schoepfi*). *Proceedings of the Royal Society of London*, 1996, **263**, 1689−1696.

[18] Harris J E. The mechanical significance of the position and movements of the paired fins in the teleostei. Papers from Tortugas Laboratory, 1937, **31**, 173−189.

[19] Webb P W. Maneuverability-general issues. *IEEE Journal of Oceanic Engineering*, 2004, **29**, 547−555.

[20] Walker J A. Kinematics and performance of maneuvering control surfaces in teleost fishes. *IEEE Journal of Oceanic Engineering*, 2004, **29**, 572−584.

[21] Weihs D. Stability versus maneuverability in aquatic locomotion. *Integrative and Comparative Biology*, 2002, **42**, 127−134.

[22] Drucker E G, Lauder G V. Wake dynamics and fluid forces of turning maneuvers in sunfish. *Journal of Experimental Biology*, 2001, **204**, 431−442.

[23] Korde U A. Study of a jet-propulsion method for an underwater vehicle. *Ocean Engineering*, 2004, **31**, 1205−1218.

[24] Park W-G, Jang J H, Chun H H, Kim M C. Numerical flow

and performance analysis of waterjet propulsion system. *Ocean Engineering*, 2005, **32**, 1740−1761.

[25] Mohseni K. Pulsatile vortex generators for low-speed maneuvering of small underwater vehicles. *Ocean Engineering*, 2006, **33**, 2209−2223.

[26] Bandyopadhyay P R. Maneuvering hydrodynamics of fish and small underwater vehicles. *Integrative and Comparative Biology*, 2002, **42**, 102−117.

[27] Blake R W. Fish functional design and swimming performance. *Journal of Fish Biology*, 2004, **65**, 1193−1222.

[28] Sfakiotakis M, Lane D M, Davies J B C. Review of fish swimming modes for aquatic locomotion. *IEEE Journal of Oceanic Engineering*, 1999, **24**, 237−252.

[29] Blake R W. On seahorse locomotion. *Journal of the Marine Biological Association of the United Kingdom*, 1976, **56**, 939−949.

[30] Breder C M, Edgerton H E. An analysis of the locomotion of the seahorse, *Hippocampus hudsonius*, by means of high speed cinematography. *Annals of the New York Academy Sciences*, 1942, **43**, 145−172.

[31] Lourie S A, Foster S J, Cooper E W T, Vincent A C J. *A Guide to the Identification of Seahorses*. Project Seahorse and TRAFFIC North America. Washington D.C.: University of British Columbia and World Wildlife Fund, 2004.

[32] Kuiter R H. *Seepferdchen, Seenadeln, Fetzenfische und ihre Verwandten Syngnathiformes*, Verlag Eugen Ulmer GmbH & Co., Stuttgart, Germany, 2001.

[33] Ashley-Ross M A. Mechanical properties of the drosal fin muscle of seahorse (Hippocampus) and pipefish (Syngnathus).*Journal of Experimental Zoology*, 2002, **293**, 561−577.

[34] Bergman R A. Mechanical properties of the dorsal fin musculature of the marine teleost, *Hippocampus hudsonius*. *Bulletin of the John Hopkins Hospital*, 1964, **114**, 344−353.

[35] Sfakiotakis M, Lane D M, Davies B C. An experimental undulating-fin device using the parallel bellows actuator. *Proceeding of the IEEE International Conference on Robotics and Automation*, Seul, Korea, 2001, **3**, 2356−2362.

[36] Lighthill M J, Blake R W. Biofluiddynamics of basilistiform and gymnotiform locomotion, Part.1, Biologycal background, and amalysis by elongated-body theory. *Journal of Fluid Mechanics*, 1990, **212**, 183−207.

[37] Daniel T, Jordan C, Grunbaum D. Hydromechanics of Swimming. *Advances in Comparative and Environmental Physiology*, 1992, **11**, 17−49.

[38] Ingard K U. *Fundamentals of Waves and Oscillations*, Cambridge University Press, Cambridge, UK, 1988.

[39] Liu H, Kawachi K. A numerical study of undulatory swimming. *Journal of Computational Physics*, 1999, **155**, 223−247.

[40] Anderson J M, Streitlien K, Barret D S, Triantafyllou M S. Oscillating foils of high propulsive efficiency. *Journal of Fluid Mechanics*, 1998, **360**, 41−72.

[41] Guglielmini L, Blondeaux P, Vittori G. A simple model of propulsive oscillating foils. *Ocean Engineering*, 2004, **31**, 883−899.

[42] Consi T R, Seifert P A, Triantafyllou M S, Edelmann E R. The dorsal fin engine of the seahorse (*Hippocampus sp.*). *Journal of Morphology*, 2001, **248**, 80−97.

[43] Wu T Y. Introduction to the scaling of aquatic animal locomotion. *Scale Effects in Animal Locomotion*(ed. Pedley T J), Academic Press, London., UK, 1977, 203−232.

[44] McHenry M J, Lauder G V. The mechanical scaling of coasting in zebrafish (*Danio rerio*). *Journal of Experimental Biology*, 2005, **208**, 2289−2301.

[45] Mittal R. Computational modelling in biohydrodynamics: Trends, challenges, and recent advances. *IEEE Journal of Oceanic Engineering*, 2004, **29**, 595−604.

[46] Gilmanov A, Sotiropoulos F. A hybrid Cartesian/immersed boundary method for simulating flows with 3D, geometrically complex, moving bodies. *Journal of Computational Physics*, 2005, **207**, 457−492.

[47] Leroyer A, Visonneau M. Numerical methods for RANSE simulations of a self-propelled fish-like body. *Journal of Fluids and Structures*, 2005, **20**, 975−991.

[48] Kim J, Kim D, Choi H. An immersed-boundary finite-volume method for simulations of flow in complex geometries. *Journal of Computational Physics*, 2001, **171**, 132−150.

[49] Kim D, Choi H. Immersed boundary method for flow around an arbitrary moving body. *Journal of Computational Physics*, 2006, **212**, 662−680.

[50] Liu W K, Liu Y, Farrell D, Zhang L, Wang X S, Fukui Y, Patankar N, Zhang Y, Bajaj C, Lee J, Hong J, Chen X, Hsu H. Immersed finite element method and its applications to biological systems. *Computer Methods in Applied Mechanics and Engineering*, 2006, **195**, 1722−1749.

[51] Patankar S V. *Numerical Heat Transfer and Fluid Flow*, Hemisphere Publishing Corporation, Washington, DC, USA, 1980.

[52] Menter F R. Zonal two-equation k-ω turbulence models for aerodynamic flows. 24*th Fluid Dynamics Conference*, Or-

lando, USA, 1993, AIAA−93−2906.

[53] Launder B E, Spalding D B. The numerical computation of turbulent flows. *Computer Methods in Applied Mechanics and Engineering*, 1974, **3**, 269−289.

[54] Wilcox D C. *The Remarkable Ability of Turbulence Model Equations to Describe Transition*, DCW Industries Inc., La Canada, CA, 1993.

[55] Wilcox D C. *Turbulence Modelling for CFD*, DCW Industries Inc., La Canada, CA, 1993.

[56] Bardina J E, Huang P G, Coakley T J. Turbulence modeling validation testing and development. *NASA Technical Memorandum* 110446, 1997.